



Structure solution of the $\text{Al}_{69.2}\text{Cu}_{20}\text{Cr}_{10.8}$ ϕ phase

 Shmuel Samuha,^{a,b} Rimon Tamari,^b Benjamin Grushko^c and Louisa Meshi^{b*}
^aNRCN, PO Box 9001, Beer-Sheva 84190, Israel, ^bDepartment of Materials Engineering, Ben Gurion University of the Negev, Beer Sheva 84105, Israel, and ^cPeter Grünberg Institut, Forschungszentrum Jülich, 52425 Jülich, Germany.

*Correspondence e-mail: lousia@bgu.ac.il

Received 7 July 2021

Accepted 10 November 2021

Edited by T. J. Sato, Tohoku University, Japan

Keywords: intermetallics; Rietveld refinement; strong-reflections approach; electron crystallography; structure prediction.

CCDC reference: 2121302

Supporting information: this article has supporting information at journals.iucr.org/j

The stable ϕ phase that forms below ~ 923 K around the $\text{Al}_{69.2}\text{Cu}_{20.0}\text{Cr}_{10.8}$ composition was found to be hexagonal [$P6_3$, $a = 11.045$ (2), $c = 12.688$ (2) Å] and isostructural to the earlier reported $\text{Al}_{6.2}\text{Cu}_2\text{Re}$ X phase [Samuha, Grushko & Meshi (2016). *J. Alloys Compd.* **670**, 18–24]. Using the structural model of the latter, a successful Rietveld refinement of the XRD data for $\text{Al}_{69.5}\text{Cu}_{20.0}\text{Cr}_{10.5}$ was performed. Both ϕ and X were found to be structurally related to the $\text{Al}_{72.6}\text{Cu}_{11.0}\text{Cr}_{16.4}$ ζ phase [$P6_3/m$, $a = 17.714$, $c = 12.591$ Å; Sugiyama, Saito & Hiraga (2002). *J. Alloys Compd.* **342**, 148–152], with a close lattice parameter c and a τ -times-larger lattice parameter a (τ is the golden mean). The structural relationship between ζ and ϕ was established on the basis of the similarity of their layered structures and common features. Additionally, the strong-reflections approach was successfully applied for the modeling of the ϕ phase based on the structural model of the ζ phase. The latter and the experimental structural model (retrieved following Rietveld refinement) were found to be essentially identical.

1. Introduction

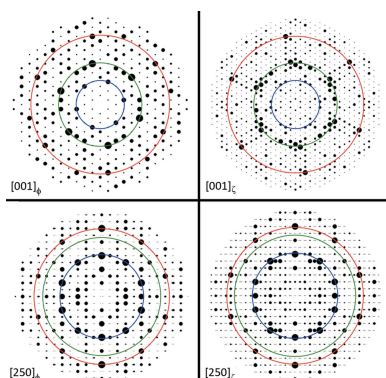
Investigation of the Al–Cu–Cr alloy system revealed several stable intermetallics, the structures of which had only been partially characterized [Grushko (2017) and references therein]. In the temperature range 843–1073 K and compositional range above 40 at.% Al, apart from the binaries, eight additional ternary compounds designated ζ , κ , ψ , S , ϕ , σ , β and Λ were revealed. The structures of the ζ phase of $\text{Al}_{72.6}\text{Cu}_{11.0}\text{Cr}_{16.4}$ and the κ phases of $\text{Al}_{67.4}\text{Cu}_{14.3}\text{Cr}_{18.3}$ were determined by single-crystal X-ray diffraction (XRD) [the latter is designated β by Sugiyama *et al.* (2002)].

In the present work we report the structure solution of the ϕ phase and its structural relationship to the ζ phase. The ϕ phase was found to form at 923 K in a small compositional region around $\sim \text{Al}_{70}\text{Cu}_{19}\text{Cr}_{11}$, while at 973 K the same composition has been associated with the S phase, whose compositional region was found to extend towards $\sim \text{Al}_{79}\text{Cu}_{10}\text{Cr}_{11}$.

The structure solution of the ϕ phase was performed by Rietveld refinement of the XRD data based on the structural model of the isostructural $\text{Al}_{6.2}\text{Cu}_2\text{Re}$ X phase (Samuha *et al.*, 2016). Additionally, a structural model of the ϕ phase was deduced from the known structure of the ζ phase using the strong-reflections approach. The two models were proved to be essentially identical. For clarity, the scheme shown in Fig. 1 presents the different phases used in the current research as well as our aim.

2. Experimental

An $\text{Al}_{69.5}\text{Cu}_{20.0}\text{Cr}_{10.5}$ alloy was produced from its constituent elements by levitation induction melting in a water-cooled



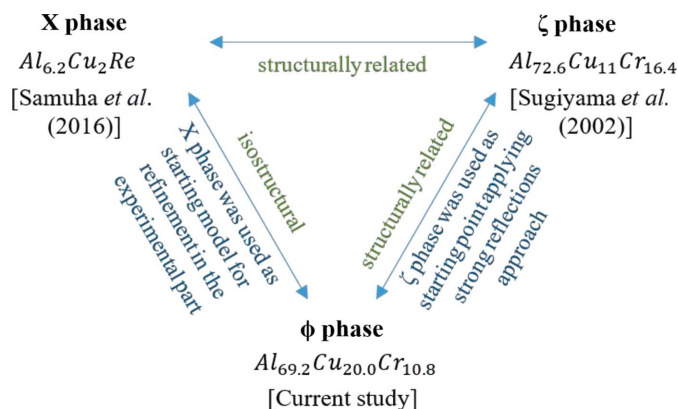


Figure 1
Scheme of the present research to illustrate the relationship between the phases studied.

copper crucible under an Ar atmosphere. The purity of Al was 99.999%, of Cu 99.95% and of Cr 99.99%. The sample was annealed under vacuum for 424 h at 923 K.

The alloy was studied by scanning electron microscopy (SEM), powder XRD and transmission electron microscopy (TEM). The compositions were analyzed by energy-dispersive X-ray analysis (EDX) with SEM. For the XRD examinations, the material was powdered in an agate mortar. The XRD pattern was recorded on a Rigaku D/MAX-2000 diffractometer equipped with a graphite monochromator with Cu $K\alpha$ radiation. The measurements were performed within the 2θ range from 5 to 100° with a step size of 0.02° and a counting rate of 10 s per step. The *FULLPROF* software (Rodriguez-Carvajal, 1998) was used to analyze the XRD data.

For the TEM examinations, the powdered material was dispersed on a grid with a carbon film. The TEM study was carried out on a FASTEM JEOL-2010 electron microscope equipped with a Nanomegas ‘Spinning Star’ precession unit. Diffraction patterns with a 120 mm camera length were recorded on a top-mounted Gatan Model 780 Dual Vision 300 camera with 1030×1300 pixels. The simulations of the precession electron diffraction (PED) patterns were performed using the program *eMAP* (Oleynikov, 2011). This program also allowed us to obtain the theoretical structure factors, calculating the 3D electron-density maps (EDMs) and extracting atomic positions from the EDMs.

3. Results and discussion

3.1. Refinement of the ϕ phase structure

The SEM examinations of the $\text{Al}_{69.5}\text{Cu}_{20.0}\text{Cr}_{10.5}$ alloy annealed at 923 K revealed a two-phase structure: the major phase with a composition close to that of the alloy and a minor phase of $\sim\text{Al}_{45.4}\text{Cu}_{53.7}\text{Cr}_{0.9}$. Since the corresponding complex powder XRD pattern could not be indexed using only known phases in this ternary system, the material was examined by electron diffraction with TEM. The corresponding PED patterns of the major ϕ phase indicated a hexagonal structure with the lattice parameters $a = 11.0$, $c = 12.75$ Å.

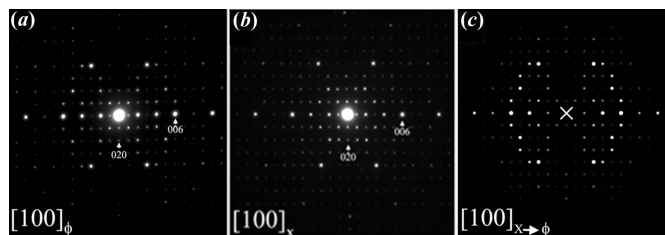


Figure 2
Experimental PED patterns along the [100] orientation of the (a) ϕ phase and (b) X phase, and (c) the corresponding PED pattern of the ϕ phase simulated using the *eMAP* software (Oleynikov, 2011). For the simulations the structural model of the ϕ phase was adopted from that of the X phase where Re was replaced by Cr.

The crystal system, unit-cell parameters and intensity distribution in the PED patterns of the ϕ phase were found to resemble those of the Al–Cu–Re X phase [$P6_3$, $a = 11.029$, $c = 12.746$ Å (Meshi *et al.*, 2009)]. For example, the PED patterns along [100] of the ϕ and X phases are compared in Figs. 2(a) and 2(b), respectively. The crystal structure of the Al–Cu–Re X phase was deduced by Samuha *et al.* (2016) through the application of direct methods on the PED tomography data and refined against the powder XRD data by the Rietveld method.

These results allowed successful indexing of the major phase in the above-mentioned powder XRD pattern. The additional reflections of the minor phase were associated with those of the Al–Cu orthorhombic phase $\zeta_{1\text{Cu}}$ [Al_3Cu_4 , *Fmm2*, $a \simeq 8.14$, $b \simeq 14.3$, $c \simeq 10.0$ Å (Gulay & Harbrecht, 2004)].¹

The ϕ and X phases are formed around quite close equivalent compositions $\text{Al}_{69.5}\text{Cu}_{20.0}\text{Cr}_{10.5}$ and $\text{Al}_{65}\text{Cu}_{25}\text{Re}_{10}$ in the Al–Cu–Cr and Al–Cu–Re phase diagrams, respectively, whereas the $\text{Al}_{6.2}\text{Cu}_2\text{Re}$ ($\text{Al}_{67.4}\text{Cu}_{21.7}\text{Cr}_{10.9}$) composition [which can be determined from the model proposed by Samuha *et al.* (2016)] is in between these two compositions. The deviation of the model composition from the measurements was ignored by Samuha *et al.* (2016). Considering the close atomic percentage of Cr and Re in these phases, the corresponding atoms could occupy the same sites, while some Cu in the X phase could be replaced by Al in the ϕ phase.

The correctness of this assumption was confirmed by the comparison of the experimental and simulated PED patterns of the ϕ phase in Figs. 2(a) and 2(c), respectively. The latter was calculated from the structural model of the Al–Cu–Re X phase, where Re was replaced by Cr, while Al and Cu were still fixed at their original positions. Figs. 2(a) and 2(c) illustrate the similar positions of the reflections (*i.e.* prove the correctness of the geometry of the unit cell), and the fact that the strongest reflections in both patterns are distributed in a

¹ The composition of the minor phase is almost binary. There are three phases in the relevant compositional region of Al–Cu. Although at the annealing temperature of 923 K the $\epsilon_{2\text{Cu}}$ phase would be expected in equilibrium with f, this was not confirmed by powder XRD. The binary $\zeta_{1\text{Cu}}$ phase is formed in a lower temperature range in the solid state, but it could be stabilized by the addition of Cr. Alternatively it could undergo transformation from $\epsilon_{2\text{Cu}}$ during cooling.

Table 1

Details of the Rietveld refinement performed on the powder XRD data taken from the studied alloy.

Parameter	Data
Structure refined	ϕ -Al _{69.2} Cu _{20.0} Cr _{10.8}
Space group	<i>P</i> 6 ₃
Unit-cell parameters (nm)	<i>a</i> = 1.0999 (5) <i>c</i> = 1.2697 (9)
Additional phases generating diffraction peaks	$\zeta_{1\text{Cu}}$ -Al ₃ Cu ₄ . Treated in profile matching mode. Only the scale factors and lattice parameters were refined.
X-ray data range (2 θ)	5.000–100.000
Zero shift	0.00157
Peak profile	Pseudo-Voigt (η = 0.87452)
Half-width parameters	<i>U</i> = 0.011425, <i>V</i> = −0.005877, <i>W</i> = 0.016688
Asymmetry parameters	<i>P</i> ₁ = 0.03012, <i>P</i> ₂ = 0.04394
Total number of reflections (of ϕ phase)	524
Reliability factors	<i>R</i> _p = 2.66, <i>R</i> _{wp} = 3.49, <i>R</i> _{exp} = 1.60, χ^2 = 4.77

Table 2

Atomic coordinates and displacement parameters for the ϕ phase structure after Rietveld refinement.

Name	Wyckoff site	<i>x</i>	<i>y</i>	<i>z</i>	<i>B</i> _{iso} (Å ²)	Occupancy
Cr1	6c	0.5682 (2)	0.9391 (3)	0.2718 (0)	0.941	1
Cr2	2b	0.3333 (3)	0.6666 (7)	0.5875 (1)	0.941	1
Cr3	2b	0.3333 (3)	0.6666 (7)	0.9357 (7)	0.941	1
Cu1	6c	0.9547 (5)	0.1964 (6)	0.0564 (8)	2.214	0.87
Al13	6c	0.9547 (5)	0.1964 (6)	0.0564 (8)	0.159	0.13
Cu2	2a	0.0000 (0)	0.0000 (0)	0.2822 (4)	2.214	1
Cu3	6c	0.9003 (4)	0.1612 (6)	0.2543 (0)	2.214	0.86
Al12	6c	0.9003 (4)	0.1612 (6)	0.2543 (0)	0.159	0.14
Cu4	6c	0.1943 (4)	0.2396 (1)	0.9618 (2)	2.152	1
Al1	6c	0.6811 (3)	0.0831 (7)	0.0745 (5)	0.159	1
Al2	6c	0.3815 (1)	0.4581 (5)	0.8754 (0)	0.159	1
Al3	6c	0.7048 (0)	0.2258 (7)	0.2746 (8)	0.159	1
Al4	6c	0.7675 (9)	0.9291 (7)	0.3640 (3)	0.159	1
Al5	6c	0.3061 (6)	0.8023 (4)	0.2356 (7)	0.159	1
Al6	6c	0.3578 (3)	0.5249 (3)	0.0700 (1)	0.159	1
Al7	6c	0.4466 (6)	0.0598 (2)	0.1542 (2)	0.159	1
Al8	6c	0.4838 (8)	0.8468 (6)	0.4356 (7)	0.159	1
Al9	6c	0.1218 (4)	0.4223 (3)	0.9457 (6)	0.159	1
Al10	6c	0.1448 (8)	0.2390 (5)	0.1566 (1)	0.159	1
Al11	2a	0.0000 (0)	0.0000 (0)	0.9981 (4)	0.159	1

similar manner and hierarchy further supports the correctness of the proposed atomic model.

Therefore, the model of the *X* phase was used as a starting point for the deduction of the structural model of the ϕ phase. It was refined by the Rietveld method on the powder XRD pattern using the *FULLPROF* software (Rodrigues-Carvajal, 1998). For convenience, the major ϕ phase was refined in Rietveld mode, while the minor $\zeta_{1\text{Cu}}$ phase was refined by applying the profile matching mode (*i.e.* refining only the geometry, without taking atom positions into account). The following parameters were refined: zero shift, lattice parameters, profile parameters, asymmetry parameters, atomic coordinates, displacement parameters and occupancy. Importantly, the last two parameter types were not refined simultaneously. First, displacement parameters were refined. After convergence, these factors were kept constant and the occupancy was refined until the program reached convergence. In the current work, an atom-type constraint was applied to the

displacement parameters (*e.g.* all Al atoms were constrained to have the same displacement parameter *etc.*).

In order to adjust the composition, which was measured by EDS as Al_{69.5}Cu_{20.0}Cr_{10.5}, one could suggest that a twofold Cu site and a twofold Al site in the model published by Samuha *et al.* (2016) would be occupied by either both Cu or both Al [the composition of the phase studied by Samuha *et al.* (2016) was Al_{65.2}Cu_{23.9}Re_{10.9} – richer in Cu and poorer in Al]. This idea was not confirmed by the refinement of the ϕ phase, which exhibited better results suggesting partial occupancy. Thus, two out of four Cu sixfold sites were suggested to be partially occupied by Al due to their position in the Cr coordination icosahedron. The details of the Rietveld refinement are summarized in Table 1; the atomic positions and displacement parameters are presented in Table 2.

The agreement factors for the refinement were *R*_p = 2.66%, *R*_{wp} = 3.49%, *R*_{Bragg} = 6.66% (of the ϕ phase) and *R*_{Bragg} = 0.788% (of Al₃Cu₄). The calculated and observed XRD profiles and the difference between them, as obtained following the refinement, are shown in Fig. 3. The interatomic distances are listed in Table 3. The occupancy refinement process led to the realistic stoichiometry of Al_{69.2}Cu_{20.0}Cr_{10.8} and exhibited convergence.

The difference in the equivalent compositions of the ϕ and *X* phases illustrates the importance of the electron concentration for the stability of these phases. To compensate the increase of the absorption of 10 electrons by ~10 Re atoms replaced by Cr, ~5 atoms of Cu (each contributing only 1 electron) should be replaced by Al (each contributing 3 electrons). Therefore, to keep the same atomic structure the ϕ phase in the Al–Cu–Cr system had to form with a different (compared with the *X* phase) stoichiometry. These effects in the resulting stable atomic structures of alluminides were thoroughly discussed by Uziel *et al.* (2015) and Yaniv *et al.* (2018, 2020). At the composition equivalent to that of the Al–Cu–Re *X* phase, the ψ phase is formed in Al–Cu–Cr, which has a different atomic structure (Grushko, 2017).

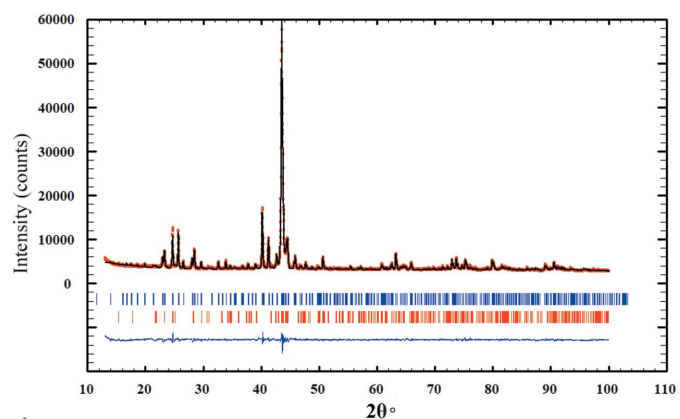


Figure 3

Plot of the Rietveld refinement of the powder XRD pattern of the Al_{69.5}Cu_{20.0}Cr_{10.5} alloy showing the observed XRD profile (red filled circles), calculated profile (black solid line) and difference between them (blue solid line). The vertical bars refer to the calculated peak positions of the ϕ phase (upper blue bars) and Al₃Cu₄ (bottom red bars).

Table 3
Interatomic distances for the ϕ phase (in Å).

CN is the coordination number. For simplicity, the coordination polyhedra of only heavy atoms are shown.

Cu4, CN = 12		Cu3 Al12, CN = 13		Cu2, CN = 13	
Al4	2.4377	Cu2	2.5333	Al4	2.4952
Al1	2.4569	Cu1 Al13	2.5663	Al4	2.4959
Al11	2.4689	Al3	2.5942	Al4	2.4961
Al2	2.5040	Al4	2.6195	Cu3 Al12	2.5333
Al9	2.5138	Al7	2.6222	Cu3 Al12	2.5337
Al10	2.5324	Al10	2.684	Al11	2.7420
Cu3 Al12	2.6863	Cu4	2.6863	Al10	2.7941
Cu1 Al13	2.7137	Al10	2.7339	Al10	2.7944
Cu1 Al13	2.7206	Al2	2.7729	Cu4	3.3287
Al4	2.8776	Al4	2.9259	Cu4	3.3288
Al6	3.0539	Al1	3.1128	Cu4	3.3290
Cu2	3.3288	Al9	3.1655		
		Cr1	3.2308		

Cu1 Al13, CN = 11		Cr3, CN = 12		Cr2, CN = 12		Cr1, CN = 12	
Al10	2.2874	Al6	2.4139	Al8	2.6658	Al8	2.2977
Al4	2.4678	Al6	2.4141	Al8	2.666	Al5	2.4454
Al7	2.5074	Al6	2.4145	Al3	2.7774	Al4	2.5363
Al11	2.5577	Al3	2.5007	Al3	2.7777	Al5	2.5387
Cu3 Al12	2.5663	Al3	2.5011	Al3	2.7778	Al2	2.705
Al1	2.6289	Al3	2.5012	Al1	2.8391	Al3	2.7328
Al9	2.6382	Al9	2.5297	Al1	2.8393	Al10	2.7467
Cu4	2.7139	Al9	2.5298	Al7	2.8882	Al7	2.7475
Cu4	2.7205	Al2	2.7096	Al7	2.8885	Al6	2.7897
Al8	3.0476	Al2	2.7099	Al7	2.8886	Al9	2.8462
Al10	3.0931	Al2	2.7105			Al1	2.8914
						Cu3 Al12	3.2311

An analysis of the simulated PED patterns of ϕ and ζ revealed similar intensity distributions of the corresponding reflections (see Fig. 4). For convenience, the positions of the exceptionally strong reflections in these patterns are emphasized using blue, green and red circles, which are the same for both phases in a particular orientation. As can be seen, the strong reflections are distributed in a similar manner along these circles in both patterns. These structures are characterized by the related space groups $P6_3$ and $P6_3/m$, respectively, and have essentially the same c lattice parameters, while their a lattice parameters (11.0 and 17.6 Å) are approximately related by τ [where $\tau = (1 + 5^{1/2})/2 \simeq 1.618$ is the golden mean]. Their structural relation is quantitatively verified below using the strong-reflections approach (Christensen, 2004, Christensen *et al.*, 2004). This approach is strictly a reciprocal space method, based on the extraction of atomic positions of the unknown structure of an approximant of a quasicrystal (approximants are defined as periodic structures having the same coordination clusters as related quasicrystals) from a 3D EDM (Shechtman *et al.*, 1984; Balanetsky *et al.*, 2004). The EDM is built using an adopted structure factor amplitude and phases of the strong reflections (which largely determine the atomic positions in a structure) from a known structure of a τ -related approximant. Use of the strongest reflections is based on the analysis of the relationship of the structure factor amplitudes and phases of reflections from a series of related quasicrystal approximants. Zhang *et al.* (2005) found that the strong reflections that are close to each other in reciprocal

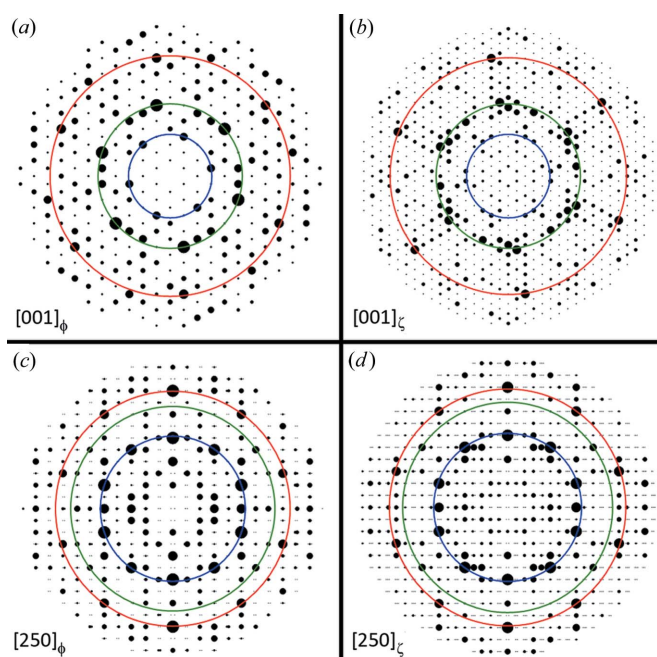


Figure 4
Simulated PED patterns along the [001] orientation and pseudo-tenfold [250] orientation of the (a), (c) ϕ phase and (b), (d) ζ phase.

space have similar structure factor amplitudes and phases for all the approximants in the series. Therefore, the structure factor amplitudes and phases of strong reflections for an unknown approximant can be estimated from those of a known related approximant. To relate the different structures, it is essential to find the orientation matrix and to re-index the reflections. The strong-reflections approach was successfully applied for structure prediction, study of the structure relationship and solution of many complex approximants (*e.g.* He *et al.*, 2007; Zhang *et al.*, 2006, 2008).

3.2. Modeling of ϕ from the structure of ζ using the strong-reflections approach

Modeling is based on the extraction of the atomic positions of a ‘target’ structure from a 3D EDM calculated by the inverse Fourier transform of the structure factor amplitudes and adopted phases of the strong reflections of a ‘related source’ structure.

For the deduction of the structure of ϕ , the reflections of ζ were ‘hand-picked’ according to the compatibility of the distribution of the strong reflections (with highest intensity in both patterns) present in the PED patterns of the two structures (see Table 4). As mentioned above, the only geometrical difference between ζ and ϕ is the length of their a lattice parameters, meaning that, for structure comparison only, a change of unit-cell dimensions is needed. Thus, the orientation matrix (A) was constructed for the re-indexing of the strongest reflections following equation (1):

$$(hkl)_\phi = \begin{pmatrix} 1/\tau & 0 & 0 \\ 0 & 1/\tau & 0 \\ 0 & 0 & 1 \end{pmatrix} (hkl)_\zeta. \quad (1)$$

Table 4

List of structure factor amplitudes and phases of the 15 strongest reflections used for the application of the strong-reflections approach.

Crystallographic information was extracted from data obtained from the work by Sugiyama *et al.* (2002).

ζ -phase strong reflections				
h	k	l	Amplitude	Phase
0	0	6	273.2	180
7	1	0	271.5	0
2	3	5	232.6	0
3	5	2	226.6	180
0	0	10	224.3	180
0	6	3	186.1	0
11	2	0	182.0	0
3	5	8	178.7	0
5	8	3	161.6	180
3	5	0	130.7	0
1	2	5	107.1	180
11	2	6	105.5	180
0	10	5	102.6	180
7	1	10	91.4	180
8	3	5	91.0	180

Using equation (1), a new set of h, k indexes of ϕ was obtained simply by re-indexing the h, k indexes of ζ ($a_\phi/a_\zeta \simeq 1.1/1.7714 \simeq 1/\tau$). Note that this procedure was only carried out for the strongest reflections of ζ which were found to be compatible (comparing the net and ideal symmetry) with those of ϕ . After re-indexing, the strongest reflections in the PED patterns of ϕ exhibited one-to-one correspondence to those of ζ (see Fig. 4). For example the strongest reflections were

$$(710)\zeta \xrightarrow{(1)} (410)\phi \quad \text{and} \quad (063)\zeta \xrightarrow{(1)} (043)\phi.$$

Next, the structure factor phases, which mainly determine the atomic positions in a structure, were modified according to their symmetry. For structurally related compounds, the relations of the structure factor phases of the strongest reflections are close (Christensen, 2004, Christensen *et al.*, 2004), which is the case for ζ and ϕ . Owing to the difference in the existence of or lack of a center of symmetry, the structure factor phases of the strongest reflections of ζ should be modified by a shift of the origin, compatible with the space group of ϕ , which is non-centrosymmetric. For this case, from comparing common

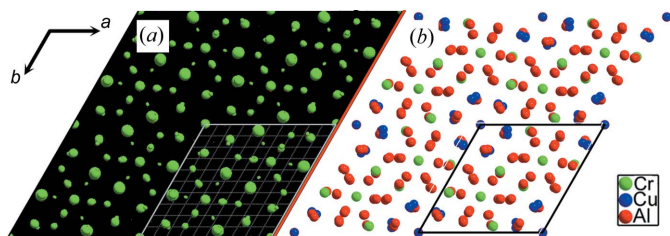


Figure 5
Deduced 3D EDM of (a) ϕ and (b) the structural model of ϕ determined experimentally, viewed along the [001] orientation. The Al, Cu and Cr atoms are marked in red, blue and green, respectively. The map consists of the spherical maxima that represent the atom positions in the unit cell, and their magnitude can be related to the atom types.

clusters (presented in the next section), the shift of the origin was found to be $(-0.34, 0.40, -0.02)$. The new structure factor phases were calculated using equation (2):

$$\phi'(hkl) = \phi'(hkl) + 360^\circ(-0.34h + 0.4k + -0.02l). \quad (2)$$

Following the shift of the origin, the phases of the symmetrically related reflections were close to those required by the symmetry of ϕ . Using *eMAP* (Oleynikov, 2011), 3D EDMs were calculated by the inverse Fourier transform of the structure factors. The calculation was based on the re-indexed strongest reflections of ζ incorporating the corresponding structure factor amplitudes and modified phases. The resulting 3D EDM viewed along the [001] orientation is shown in Fig. 5(a). Following the ‘peak hunting’ procedure in *eMAP* (Oleynikov, 2011), the full theoretical model of ϕ was obtained. Thus, using a limited number of strong reflections, a successful deduction of the structure model of ϕ , based on that of ζ , was achieved. Comparison of the experimental structure of ϕ [Fig. 5(b)] with that deduced from ζ shows a close similarity. Using the *Compstru* software (Tasci *et al.*, 2012) for a quantitative comparison of the atomic models (*i.e.* the model listed in Table 2 determined using the Rietveld refinement) with those derived applying the strong-reflections approach, the measure of similarity (Bergerhoff *et al.*, 1999) was found to be $\Delta = 0.04$ with the largest interatomic distance $d = 0.56 \text{ \AA}$, meaning essential identity.

3.3. Family of τ -related hexagonal structures in Al-based alloy systems

Although the ϕ -type structure was only revealed in the Al–Cu–Cr (or Re) alloy systems, the ζ -type structure is also known in Al–Cr–Ni (Grushko *et al.*, 2008), Al–Cr–Pd (Kowalski *et al.*, 2010) and Al–Mn–Co (or Ni, or Fe) (Grushko *et al.*, 2016). In addition to this family, there is a hexagonal λ -Al₄Mn structure [*P*6₃/*m*, $a = 28.382, c = 12.4 \text{ \AA}$ (Kreiner & Franzen, 1997)] with the lattice parameter c close to those of ϕ and ζ and the lattice parameter a about τ times larger than that of ζ . All this points to a large family of related phases.

Both ϕ and ζ can be represented as a six-layered structure perpendicular to the c axis (see Fig. 6). The common description of their layers includes type and packing: there are two approximately flat layers (designated F and f) and four puckered thick layers (designated P, P', p, p'). The layers are

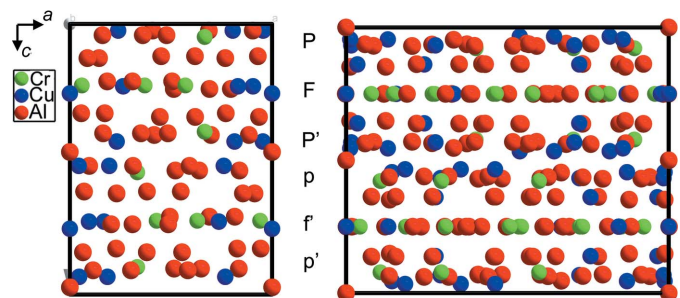


Figure 6
Structures of ϕ (left) and ζ (right) projected along the [010] orientation.

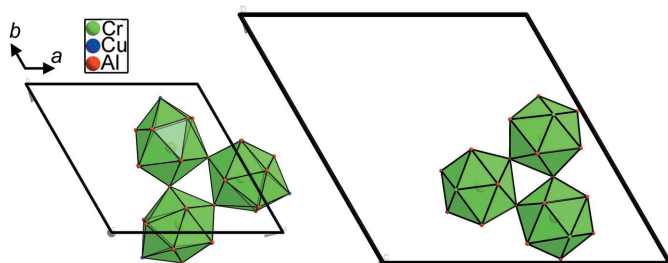


Figure 7
I3 cluster in the structures of ϕ (left panel) and ζ (right panel) projected along the [010] orientation.

organized in the PFP'pfp' sequence, where the PFP' layers are related by a 2_1 screw axis to the pfp' layers. In the ϕ structure, the puckered layers consist of atoms that are arranged as if a pseudo-mirror exists in each of the flat layers. The only difference between the ϕ and the ζ structures, in this respect, is that the latter can be regarded as a mirror rather than a pseudo-mirror, as a result of the higher symmetry of ζ ($P6_3/m$ versus $P6_3$).

The atoms in ϕ have similar icosahedral coordination. The I3 cluster (Kreiner & Franzen, 1997; Mo & Kuo, 2000) is of particular interest. It is constructed from three icosahedra built around the Cr atoms positioned in the flat layers. Since this cluster is not only present but also distributed in a similar manner in both structures, it can be regarded as the fundamental structural unit. The position of this cluster (presented in Fig. 7) in both structures is identical if a shift of the origin to $(-0.34, 0.40, -0.02)$ is introduced. These facts provide proof from real space for the correctness of the atomic model and structural relationship, as there are many structural similarities between the structures of ϕ and ζ , mainly in their fundamental building blocks and layers.

4. Conclusions

Rietveld refinement of the powder XRD data for the $\text{Al}_{69.5}\text{Cu}_{20.0}\text{Cr}_{10.5}$ ϕ phase [$P6_3$, $a = 11.045$ (2), $c = 12.688$ (2) Å] was successfully performed on the basis of the structural model of the isostructural $\text{Al}_{6.2}\text{Cu}_2\text{Re}$ X phase. Using the strong-reflections approach, these phases were found to be structurally related to the $\text{Al}_{72.6}\text{Cu}_{11.0}\text{Cr}_{16.4}$ ζ phase ($P6_3/m$, $a = 17.714$, $c = 12.591$ Å) with a close lattice parameter c and a τ -times-larger lattice parameter a (τ is the golden mean).

Structural similarities between the ζ and ϕ phases support their affiliation to the same family of τ -related phases.

Acknowledgements

The authors thank C. Thomas for alloy preparation.

References

- Balanetsky, S., Grushko, B. & Velikanova, T. Y. (2004). *Z. Kristallogr. Cryst. Mater.* **219**, 779–781.
- Bergerhoff, G., Berndt, M., Brandenburg, K. & Degen, T. (1999). *Acta Cryst.* **B55**, 147–156.
- Christensen, J. (2004). Licentiate thesis, Stockholm University, Sweden.
- Christensen, J., Oleynikov, P., Hovmöller, S. & Zou, S. (2004). *Ferroelectrics*, **305**, 273–277.
- Grushko, B. (2017). *J. Alloys Compd.* **729**, 426–437.
- Grushko, B., Kowalski, W., Pavlyuchkov, D., Przepiórzyński, B. & Surowiec, M. (2008). *J. Alloys Compd.* **460**, 299–304.
- Grushko, B., Pavlyuchkov, D., Mi, S. & Balanetsky, S. (2016). *J. Alloys Compd.* **677**, 148–162.
- Gulay, L. D. & Harbrecht, B. (2004). *J. Alloys Compd.* **367**, 103–108.
- He, Z. B., Zou, X. D., Hovmöller, S., Oleynikov, P. & Kuo, K. H. (2007). *Ultramicroscopy*, **107**, 495–500.
- Kowalski, W., Grushko, B., Pavlyuchkov, D. & Surowiec, M. (2010). *J. Alloys Compd.* **496**, 129–134.
- Kreiner, G. & Franzen, H. F. (1997). *J. Alloys Compd.* **261**, 83–104.
- Meshi, L., Grushko, B. & Ezersky, V. (2009). *J. Alloys Compd.* **488**, 108–111.
- Mo, Z. M. & Kuo, K. H. (2000). *Mater. Sci. Eng. A*, **294–296**, 242–245.
- Oleynikov, P. (2011). *Cryst. Res. Technol.* **46**, 569–579.
- Rodriguez-Carvajal, J. (1998). *FULLPROF*, Version 0.2. Laboratoire Léon Brillouin, Saclay, France.
- Samuha, S., Grushko, B. & Meshi, L. (2016). *J. Alloys Compd.* **670**, 18–24.
- Shechtman, D., Blech, I., Gratias, D. & Cahn, J. W. (1984). *Phys. Rev. Lett.* **53**, 1951–1953.
- Sugiyama, K., Saito, H. & Hiraga, K. (2002). *J. Alloys Compd.* **342**, 148–152.
- Tasci, E. S., de la Flor, G., Orobengoa, D., Capillas, C., Perez-Mato, J. M. & Aroyo, M. I. (2012). *EPJ Web Conf.* **22**, 9.
- Uziel, A., Bram, A. I., Venkert, A., Kiv, A. E., Fuks, D. & Meshi, L. (2015). *J. Alloys Compd.* **648**, 353–359.
- Yaniv, G., Fuks, D. & Meshi, L. (2018). *Intermetallics*, **100**, 44–51.
- Yaniv, G., Vidal, D., Fuks, D. & Meshi, L. (2020). *Metals*, **10**, 422.
- Zhang, H., He, Z. B., Oleynikov, P., Zou, X. D., Hovmöller, S. & Kuo, K. H. (2006). *Acta Cryst.* **B62**, 16–25.
- Zhang, H., Wang, S. J., Wang, S. C., Li, Z. C., Hovmöller, S. & Zou, X. D. (2008). *J. Comput. Theor. Nanosci.* **5**, 2.
- Zhang, H., Zou, X. D., Oleynikov, P. & Hovmöller, S. (2005). *Philos. Mag.* **86**, 5.